

## Direct experimental evidence of hybridization of Pb states with O 2p states in ferroelectric perovskite oxides

J. C. Jan,<sup>a)</sup> H. M. Tsai, C. W. Pao, J. W. Chiou, K. Asokan,<sup>b)</sup>  
K. P. Krishna Kumar, and W. F. Pong<sup>c)</sup>

*Department of Physics, Tamkang University, Tamsui, Taiwan 251, Republic of China*

Y. H. Tang and M.-H. Tsai

*Department of Physics, National Sun Yat-Sen University, Kaohsiung, Taiwan 804, Republic of China*

S. Y. Kuo

*Precision Instrument Development Center, National Science Council, Hsinchu, Taiwan 300, Republic of China*

W. F. Hsieh

*Department of Photonics and Institute of Electro-Optical Engineering, National Chiao Tung University, Hsinchu, Taiwan 300, Republic of China*

(Received 10 March 2005; accepted 25 May 2005; published online 28 June 2005)

This work presents the O *K*- and Ti *L*<sub>3,2</sub>-edge x-ray absorption near-edge structure (XANES) spectra of Pb<sub>x</sub>Sr<sub>1-x</sub>TiO<sub>3</sub> (P<sub>x</sub>STO) and Ba<sub>x</sub>Sr<sub>1-x</sub>TiO<sub>3</sub> (B<sub>x</sub>STO) compounds with various Pb and Ba concentrations. The result provides direct evidence that the Pb–O bonding strongly affects O 2p–Ti 3d hybridization in the TiO<sub>6</sub> octahedron of P<sub>x</sub>STO. In contrast, the Ba–O bonding does not substantially affect O 2p–Ti 3d hybridization in B<sub>x</sub>STO. The Ti *L*<sub>3</sub>-edge XANES spectra show the splitting of the *e*<sub>g</sub> band for P<sub>x</sub>STO with *x* ≥ 0.5, which provides an evidence of Pb-induced tetragonal distortion in the TiO<sub>6</sub> octahedron. In contrast, *e*<sub>g</sub> band splitting is absent in B<sub>x</sub>STO. © 2005 American Institute of Physics. [DOI: 10.1063/1.1988984]

Ferroelectric perovskite oxides of the ABO<sub>3</sub>-type including BaTiO<sub>3</sub> (BTO), SrTiO<sub>3</sub> (STO), and PbTiO<sub>3</sub> (PTO) are important materials because of their piezoelectric, pyroelectric and dielectric properties.<sup>1,2</sup> Interestingly, these materials have tunable properties over a wide range of mixed solid solutions doped with various cations.<sup>1</sup> A characteristic unit cell of these perovskites contains a TiO<sub>6</sub> octahedron. Collective polarization of the TiO<sub>6</sub> octahedra is believed to determine the ferroelectric characteristics.<sup>3–6</sup> X-ray absorption near-edge structure (XANES) measurements and first-principles calculations have been used to elucidate the role of alkaline-earth metals in perovskites,<sup>7–9</sup> which showed that A cations influenced the coupling between Ti and O ions and is responsible for tuning the ferroelectric properties. Kuo *et al.* determined the lattice constant from x-ray diffraction (XRD) data and observed a structural change from cubic to tetragonal (associated with an increase in the tetragonal distortion *c/a*) for Pb<sub>x</sub>Sr<sub>1-x</sub>TiO<sub>3</sub> (P<sub>x</sub>STO) at *x*=0.5 (Ref. 10) and for Ba<sub>x</sub>Sr<sub>1-x</sub>TiO<sub>3</sub> (B<sub>x</sub>STO) at *x*=0.7.<sup>11</sup> They also carried out Raman measurements for P<sub>x</sub>STO and B<sub>x</sub>STO and found that the splitting of longitudinal optical (LO) and transverse optical (TO) modes became stronger as the Pb content in the tetragonal phase of P<sub>x</sub>STO increases, while the splitting became weaker as the Ba content in B<sub>x</sub>STO increases. These results were explained by the covalent Pb–O bonding in P<sub>x</sub>STO and ionic Ba–O bonding in B<sub>x</sub>STO.<sup>10–12</sup> The present study is intended to understand the electronic structures of P<sub>x</sub>STO and

B<sub>x</sub>STO solid solutions by O *K*- and Ti *L*<sub>3,2</sub>-edges XANES measurements to elucidate the role of Pb and Ba ions in M<sub>x</sub>Sr<sub>1-x</sub>TiO<sub>3</sub> (M=Pb and Ba).

Room-temperature XANES spectra at the O *K*- and Ti *L*<sub>3,2</sub>-edges were recorded using a high-spherical grating monochromator beamline in fluorescence and sample drain current modes, respectively, at the National Synchrotron Radiation Research Centre, Taiwan. P<sub>x</sub>STO and B<sub>x</sub>STO (where *x* is varied from 0 to 1) solid solutions were prepared by the sol-gel method and characterized by XRD. The details of the preparation and characterization of these samples have been reported elsewhere.<sup>10,11</sup>

Figures 1 and 2 present the normalized O *K*-edge XANES spectra of P<sub>x</sub>STO and B<sub>x</sub>STO (*x*=0 to 1) compounds, respectively, and reference TiO<sub>2</sub>. These spectra were divided by the incident intensity *I*<sub>0</sub> and normalized to the same area in the energy range between 550 and 560 eV (not fully shown). The main spectral features in the spectra of PTO (BTO) in Fig. 1 (Fig. 2) are centered at ~531 (530.5), 532, 534 (533.5), and 537 (537) eV and are labeled as A<sub>1</sub> (A<sub>2</sub>) to D<sub>1</sub> (D<sub>2</sub>), respectively. These features correspond to transitions from the O 1s core state to the unoccupied O 2p-derived states. According to first-principles calculations for P<sub>x</sub>STO (Ref. 13) and B<sub>x</sub>STO (Ref. 9) these states are hybridized states between O 2p and relatively narrow 3d and broader 4sp bands of the Ti ion and Pb 6sp and Sr 4d/(Ba 5d) bands. Specifically, spectral features A<sub>1</sub>, C<sub>1</sub>, and B<sub>1</sub> are attributable to hybridized states between O 2p and Ti 3d and Pb 6sp, while features A<sub>2</sub> and C<sub>2</sub> are associated with O 2p–Ti 3d hybridized states. A similar two-peak structure (*t*<sub>2g</sub> and *e*<sub>g</sub> states) at the threshold of the O *K*-edge is commonly obtained from 3d-transition metal oxides.<sup>14</sup> Feature D<sub>1</sub> (D<sub>2</sub>) in the spectra of P<sub>x</sub>STO (B<sub>x</sub>STO) is attributable

<sup>a)</sup>Present address: National Synchrotron Radiation Research Center, Hsinchu, Taiwan 300, Republic of China.

<sup>b)</sup>Permanent address: Nuclear Science Centre, Aruna Asaf Ali Marg, New Delhi-110067, India.

<sup>c)</sup>Author to whom correspondence should be addressed; electronic mail: wfpong@mail.tku.edu.tw

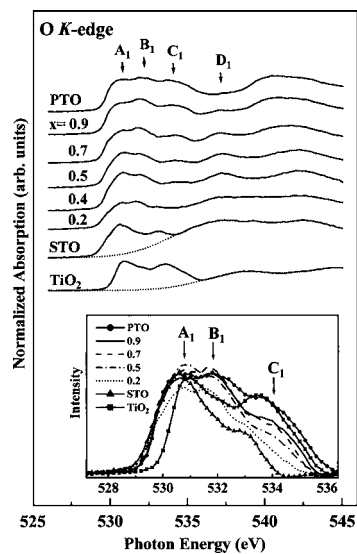


FIG. 1. Normalized O *K*-edge XANES spectra of the  $P_x\text{STO}$  ( $x=0-1$ ) samples. The dashed line represents a best-fitted Gaussian shape background. The inset shows the magnified near-edge feature after background subtraction.

to the O  $2p$  derived states hybridized with Sr  $4d$  (Sr  $4d$ /Ba  $5d$ ) orbitals. The insets of Figs. 1 and 2 show magnified near-edge features with the background subtracted to highlight intensity differences. The inset of Fig. 1 shows that feature  $B_1$  emerges between features  $A_1$  and  $C_1$  when the Pb content is added. Furthermore, strong hybridization between O  $2p$  and Ti  $3d$ /Pb  $6sp$  states increases the number of unoccupied O  $2p$  derived states and broadens the features for  $P_x\text{STO}$ . In contrast, the general spectral line shapes and widths in the inset of Fig. 2 are very similar for  $B_x\text{STO}$  because Ba and Sr ions have similar valence states. The similarity of the spectra of  $B_x\text{STO}$  also shows that substitution of Sr by Ba insignificantly affects the Ti–O bonding in  $B_x\text{STO}$ . Feature  $A_2$  shifts slightly to lower energy as the Ba content increases. This trend is due to the fact that the electronegativity of Ba (0.89) is slightly less than that of Sr (0.95),<sup>15</sup> so that the average electronegativity of cations decreases and

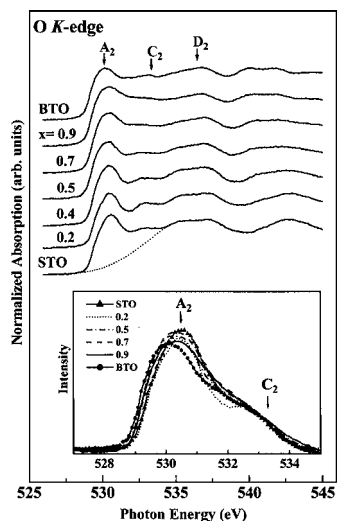


FIG. 2. Normalized O *K*-edge XANES spectra of the  $B_x\text{STO}$  ( $x=0-1$ ) samples. The dashed line represents a best-fitted Gaussian shape background. The inset shows the magnified near-edge feature after background subtraction.

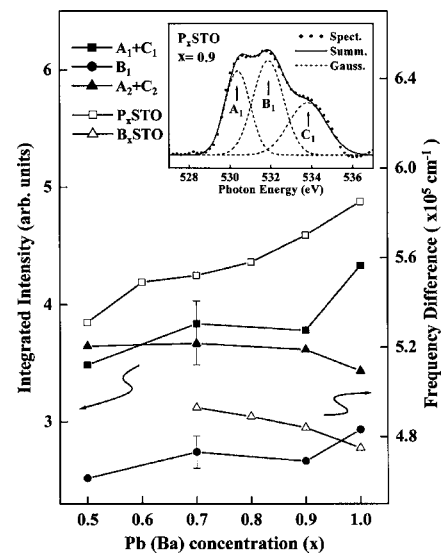


FIG. 3. Integrated intensities of  $A_1+C_1$ ,  $B_1$ , and  $A_2+C_2$  features in O *K*-edge XANES spectra as functions of the Pb (Ba) concentration. [The frequency difference data of  $P_x\text{STO}$  (open squares) and  $B_x\text{STO}$  (open triangles) are from Refs. 10 and 11, respectively]. The inset shows a magnified view of  $A_1$ ,  $B_1$ , and  $C_1$  features and fitted result of  $P_x\text{STO}$  at  $x=0.9$ .

the negative effective charge of the O ion increases with the Ba content. The O *K*-edge XANES spectra of  $P_x\text{STO}$  have more features than those of  $B_x\text{STO}$ . This indicates that the Pb–O covalent bonding has additional contribution to the spectra and such result is consistent with the findings of Kuroiwa *et al.*<sup>16</sup> and also in agreement with the theoretical prediction of Cohen.<sup>4</sup>

Figure 3 plots the integrated intensities of  $A_1+C_1$  (ranged from 528 to 532 eV and 532 to 536 eV, respectively),  $B_1$  (ranged from 530 to 534 eV), and  $A_2+C_2$  (ranged from 528 to 535 eV) absorption features attributable to O  $2p$ –Ti  $3d$  and O  $2p$ –Pb  $6sp$  derived states, respectively, as a function of the Pb (Ba) concentration in  $P_x\text{STO}$  ( $B_x\text{STO}$ ). The inset of Fig. 3 shows a magnified view after background subtraction to better resolve  $A_1$ ,  $B_1$ , and  $C_1$  features of  $P_x\text{STO}$  using the  $x=0.9$  case as an example. Three best-fitted Gaussian peaks are used to represent  $A_1$ ,  $B_1$ , and  $C_1$  features. Figure 3 also compares the frequency difference between TO[ $A_1(\text{TO}_1)$ ] and LO[ $A_1(\text{LO}_3)$ ] as a function of the Pb (Ba) concentration from Refs. 10 and 11. Figure 3 demonstrates that the partial substitution of A cations, Sr, by Pb increases the number of unoccupied O  $2p$ –Ti  $3d$  and O  $2p$ –Pb  $6sp$  hybridized states when  $x$  increases from 0.5 to 1 in  $P_x\text{STO}$ , which may suggest a charge transfer that increases the effective charges of Ti and, consequently, the attractive Coulomb potentials on Ti sites (Pb has a much larger electronegativity than Ti and Sr, so its effective charge is less likely to increase). This charge transfer causes the LO–TO splitting to increase with the Pb content in  $P_x\text{STO}$ . In contrast, Fig. 3 reveals that the overall intensities of the sum of features of  $A_2$  and  $C_2$  drops slightly as the Ba content increases, which indicates a decrease of the number of unoccupied O  $2p$ –Ti  $3d$  hybridized states and suggests a reduction of the effective charge that decreases the Coulomb force between O and Ti ions and, consequently, a slight decrease of the LO–TO splitting in  $B_x\text{STO}$ . The ferroelectric property results from a detailed balance between the long-range Coulomb interaction and short-range forces.<sup>4</sup> Thus, the significant charge transfer in  $P_x\text{STO}$  enhances the long-range Cou-

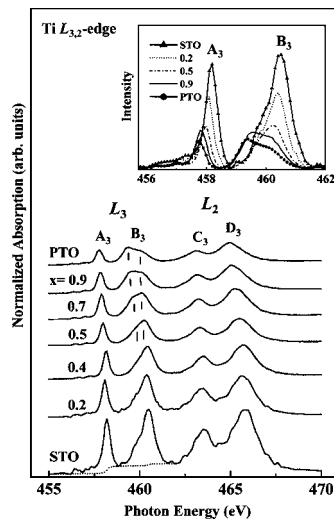


FIG. 4. Normalized Ti  $L_{3,2}$ -edge XANES spectra of  $P_x$ STO. The inset presents the magnified  $A_3$  and  $B_3$  features after background subtraction.

lomb interaction and improves the ferroelectric characteristics.

Figures 4 and 5 present the Ti  $L_{3,2}$ -edge XANES spectra of  $P_x$ STO and  $B_x$ STO compounds, respectively. These spectra are split into  $L_3$  and  $L_2$  regions by the spin-orbit interaction in the Ti  $2p$  core states<sup>17–19</sup> with a separation of  $\sim 5.5$  eV. Each region contains  $t_{2g}$  and  $e_g$  splitting of approximately 2 eV caused by the crystal-field effect. The spectra in Fig. 4 contain four dominant features, of which the first two features,  $A_3$  and  $B_3$ , correspond to the  $L_3$ -edge with  $t_{2g}$  and  $e_g$  symmetries, respectively. The other two features,  $C_3$  and  $D_3$ , in the higher-energy region correspond to the  $L_2$ -edge with  $t_{2g}$  and  $e_g$  symmetries, respectively.<sup>19,20</sup> The crystal field due to the perfect  $O_h$  symmetry gives rise to two distinct  $t_{2g}$  and  $e_g$  bands. The lowering of the symmetry to  $D_{2d}$  causes  $e_g$  to split. Feature  $B_3$  exhibits a splitting of approximately 0.5 eV (marked by the vertical lines in Fig. 4) for  $P_x$ STO for  $x \geq 0.5$ , which suggests off-center displacement of the Ti ion. This splitting can be understood by the strong tetragonal distortion.<sup>8</sup> In contrast, as presented in Fig. 5, feature  $B_4$  in the spectra of  $B_x$ STO exhibits no clear splitting, which indicates that the tetragonal distortion  $c/a$  is in-

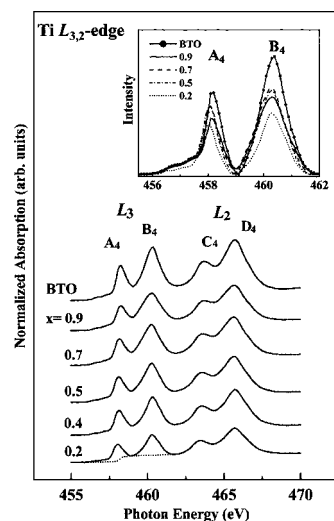


FIG. 5. Normalized Ti  $L_{3,2}$ -edge XANES spectra of  $B_x$ STO. The inset presents the magnified  $A_4$  and  $B_4$  features after background subtraction.

significant for  $B_x$ STO.<sup>11</sup> The insets of Figs. 4 and 5 highlight the splitting by subtracting the background using two arc-tangent functions shown by dashed lines. These two arc-tangent functions, which represent the atomiclike absorption step functions, are related to the ionization potentials<sup>21</sup> associated with the excitation of  $2p$  electrons to the unoccupied  $3d$  states at the Ti site.

The intensity decreases and the energy shifts to lower energies as  $x$  increases, suggesting that the effective charge of the Ti ion increases in  $P_x$ STO. This finding reflects that Pb has a larger electronegativity than Ti (2.33 vs. 1.54),<sup>15</sup> so that there is electron transfer from Ti to Pb, which increases the positive effective charge of Ti. In contrast, the spectra of  $B_x$ STO after background subtraction reveal that the intensity of the  $L_3$ -edge feature overall increases as the Ba content increases as shown in the inset of Fig. 5, which suggests that the Ti effective charge decrease with the increase of the Ba content. In this case, the decrease of the Ti effective charge reflects the smaller electronegativity of Ba than Ti (0.89 versus 1.54);<sup>15</sup> the direction of electron transfer is from Ba to Ti, which reduces the positive effective charge of Ti.

In summary, the XANES measurements provide direct evidence that the Pb–O bonding strongly affects O  $2p$ –Ti  $3d$  hybridization in the  $TiO_6$  octahedron of  $P_x$ STO. In contrast, the Ba–O bonding does not substantially affect O  $2p$ –Ti  $3d$  hybridization in  $B_x$ STO. The Ti  $L_3$ -edge XANES spectra provide evidence of Pb-induced tetragonal distortion in the  $TiO_6$  octahedron for  $x \geq 0.5$ . In contrast, this effect is absent in  $B_x$ STO.

This work was supported by National Science Council (NSC) of Republic of China under Contract No. NSC 93-2112-M-032-018.

<sup>1</sup>For example, see M. E. Lines, and A. M. Glass, *Principles and Applications of Ferroelectrics and Related Materials* (Clarendon, Oxford, 1979); J. F. Scott and C. A-Paz de Araujo, *Science* **246**, 1400 (1989).

<sup>2</sup>S. Piskunov, E. Heifets, R. I. Eglitis, and G. Borstel, *Comput. Mater. Sci.* **29**, 165 (2004).

<sup>3</sup>C. Kittel, *Introduction to Solid State Physics*, 7th ed. (Wiley, New York, 1996).

<sup>4</sup>R. E. Cohen, *Nature (London)* **358**, 136 (1992).

<sup>5</sup>B. Ravel, Ph.D. thesis, University of Washington, 1997.

<sup>6</sup>M. Imada, A. Fujimori, and Y. Tokura, *Rev. Mod. Phys.* **70**, 1039 (1998).

<sup>7</sup>K. Asokan, J. C. Jan, J. W. Chiou, W. F. Pong, M.-H. Tsai, H. L. Shih, H. Y. Chen, H. C. Hsueh, C. C. Chuang, Y. K. Chang, Y. Y. Chen, and I. N. Lin, *J. Phys.: Condens. Matter* **13**, 11087 (2001).

<sup>8</sup>J. C. Jan, K. Kumar, J. W. Chiou, H. M. Tsai, H. L. Shih, H. C. Hsueh, S. C. Ray, K. Asokan, W. F. Pong, M.-H. Tsai, S. Y. Kuo, and W. F. Hsieh, *Appl. Phys. Lett.* **83**, 3311 (2003).

<sup>9</sup>Y. H. Tang, M.-H. Tsai, J. C. Jan, and W. F. Pong, *Chin. J. Phys. (Taipei)* **41**, 167 (2003).

<sup>10</sup>S. Y. Kuo, C. T. Li, and W. F. Hsieh, *Appl. Phys. Lett.* **81**, 3019 (2002).

<sup>11</sup>S. Y. Kuo, W. Y. Liao, and W. F. Hsieh, *Phys. Rev. B* **64**, 224103 (2001).

<sup>12</sup>S. Y. Kuo, C. T. Li, and W. F. Hsieh, *Phys. Rev. B* **69**, 184104 (2004).

<sup>13</sup>Y. H. Tang and M.-H. Tsai (unpublished).

<sup>14</sup>F. M. F. de Groot, M. Grioni, J. C. Fuggle, J. Ghijsen, G. A. Sawatzky, and H. Petersen, *Phys. Rev. B* **40**, 5715 (1989).

<sup>15</sup>*Table of Periodic Properties of the Elements* (Sargent-Welch Scientific, Skokie, Illinois, 1980).

<sup>16</sup>Y. Kuroiwa, S. Aoyagi, A. Sawada, J. Harada, E. Nishibori, M. Takata, and M. Sakata, *Phys. Rev. Lett.* **87**, 217601 (2001).

<sup>17</sup>F. M. F. de Groot, M. Grioni, B. T. Thole, G. A. Sawatzky, and J. C. Fuggle, *Phys. Rev. B* **41**, 928 (1990).

<sup>18</sup>M. Abbate, R. Potze, G. A. Sawatzky, C. Schlenker, H. J. Lin, L. H. Tjeng, C. T. Chen, D. Teehan, and T. S. Turner, *Phys. Rev. B* **51**, 10150 (1995).

<sup>19</sup>J. P. Crocombette and F. Jollet, *J. Phys.: Condens. Matter* **6**, 10811 (1994).

<sup>20</sup>G. van der Laan, *Phys. Rev. B* **41**, 12366 (1990).

<sup>21</sup>J. Stöhr, *NEXAFS Spectroscopy* (Springer, Berlin, 1992), p. 231.